Chaos

AIP Publishing

Using critical curves to compute master stability islands for amplitude death in networks of delay-coupled oscillators

Stanley R. Huddy[1, a)]
Gildart Haase School of Computer Sciences and Engineering, Fairleigh Dickinson University, 1000 River Road, Teaneck, NJ 07666, USA

(Dated: 17 December 2019)

In this paper, we present a method to compute master stability islands (MSIs) for amplitude death (AD) in networks of delay-coupled oscillators using critical curves. We first demonstrate how critical curves can be used to compute boundaries and contours of MSIs in delay-coupling parameter space, and then provide a general study on the effects of the oscillator dynamics and network topology on the number, size, and contour types of all MSIs. We find that the oscillator dynamics can be used to determine the number and size of MSIs and that there are six possible contour types that depend on the choice of oscillator dynamics and the network topology. We introduce contour sequences and use these sequences to study the contours of all MSIs. Finally, we provide example MSIs for several classical nonlinear systems including: the van der Pol system, the Rucklidge system, and the Rössler system.

Many naturally-occurring systems oscillate, and oscillator models provide a mathematical descriptor of their processes. Because oscillating systems frequently interact, networks of oscillators are implemented to model these interactions and describe their collective behavior. To account for finite propagation times of information in real-world settings, researchers incorporate delay in the communication between systems, creating networks of delay-coupled oscillators. Understanding the dynamic behaviors and synchronization patterns displayed on these networks provides invaluable insight into the collective behavior of interacting real-world systems. In this paper, we study the dynamic behavior of amplitude death, which occurs when coupling interactions cause the oscillatory behavior of a network to gradually cease. We provide a method to identify the delay and coupling values that result in amplitude death in a network.

I. INTRODUCTION

Amplitude death (AD) is a dynamic phenomenon observed in networks of oscillators. AD occurs when the collective network dynamics decay (synchronize) onto a stabilized homogeneous fixed point of the uncoupled oscillator dynamics. AD has been observed in a wide range of networks with homogeneous or heterogeneous node dynamics using a variety of coupling schemes[1–24]. When AD occurs in networks of delay-coupled oscillators, there exists enclosed regions in delay and coupling constant parameter space corresponding to stable AD in the network[16–24]. These regions are called amplitude death islands (ADIs) and it has been shown that the number and size of these islands depend on the choice of oscillator and the network topology. Because ADIs provide delay and coupling constant parameter pairings that result in stable AD, researchers can use these islands to induce AD[25] or avoid AD[22,23] in a coupled system.

a)Electronic mail: srh@fdu.edu.

Another way to represent regions of stable AD for networks of delay-coupled oscillators is to use master stability islands (MSIs)[26]. MSIs are stability surfaces, defined by a master stability function, that provide regions of stable AD for all possible networks for a fixed choice of oscillator dynamics. Like ADIs, MSIs can be visualized as enclosed regions in delay and coupling parameter space. Each region represents where it is possible to observe stable AD for networks with the chosen oscillator dynamics, and contour lines are added to each region to indicate the network specific subregions of stable AD. A major benefit of using MSIs to visualize regions of stable AD is that, once they are computed for the chosen oscillator dynamics, they can be used to determine the region of stable AD for any network with those node dynamics. Studies that utilize ADIs often compute islands for multiple networks with the same oscillator dynamics[21,23], but MSIs are a more efficient way to do this, as they do not need to be newly generated for each different network topology. ADIs and MSIs can be computed using the Lambert W function[26], and in this paper, we present a way to compute MSIs using four critical curves that are found in the AD literature[16–19,21].

In Sec. II, we give the network model, present linear stability analysis of the AD solution, and define the critical curves. In Sec. III, we discuss how to use the critical curves to compute MSIs. We show how the first two critical curves can be used to compute the boundaries of the MSIs corresponding to any choice of oscillator dynamics. We find that the number of MSIs and their corresponding sizes depend solely on the chosen oscillator dynamics, that all of the resulting MSIs share a common minimum coupling value, and that we can compute a curve that intersects the maximum coupling value of each MSI. Next, we show how the second two critical curves can be used to compute contours inside each MSI. In Sec. IV, we show that there are only six possible MSI contour types, and we analyze how the oscillator dynamics and network topology affect which of the six contour types that are found inside any MSI. We also define horizontal and vertical contour sequences and use these sequences to describe the contour types of all MSIs. In Sec. V, we give examples of MSIs for several classical nonlinear systems including the van der Pol system, the Rucklidge system, and the Rössler system, and we use

the vertical contour sequences to describe the possible contour types of each MSI. Finally, in Sec. VI, we discuss our results and the conclusions that can be drawn from our work.

II. STABILITY OF AMPLITUDE DEATH

We consider a general undirected network of n identical oscillators with linear delay-coupling and write the dynamics of the ith node as

$$\dot{\mathbf{x}}_i(t) = F(\mathbf{x}_i(t)) + \sigma \sum_{j=1}^{n} g_{ij}(\mathbf{x}_j(t-\tau) - \mathbf{x}_i(t)), \qquad (1)$$

where $\mathbf{x}_i(t) \in \mathbb{R}^m$ is the state of the node i at time t, $F(\mathbf{x}_i(t)) : \mathbb{R}^m \to \mathbb{R}^m$ is the oscillator dynamics of node i, σ is the network coupling constant, and $\tau > 0$ is a constant delay. The matrix $G = [g_{ij}]_{n\times n}$ is the network coupling matrix, where $g_{ij} = 1/\sum_{j=1}^{n} g_{ij}$ if node i is coupled to node j for $i \neq j$, and $g_{i,j} = 0$ otherwise. By definition, G is symmetric and each of its rows sum to one. Thus, the eigenvalues of G satisfy $\gamma_i \in [-1, 1]$, where the largest eigenvalue is always $\gamma_1 = 1$ and the smallest eigenvalue γ_n satisfies[21,27]

$$-1 \leq \gamma_n \leq -\frac{1}{n-1} < 0.$$

The AD phenomenon is observed in the network when

$$\mathbf{x}_1(t) = \mathbf{x}_2(t) = \cdots = \mathbf{x}_n(t) = \mathbf{x}^*,$$

where $\mathbf{x}^*$ is an unstable fixed point of the chosen oscillator dynamics satisfying $F(\mathbf{x}^*) = 0$. We consider the case where $DF(\mathbf{x}^*)$ has conjugate eigenvalues $\alpha \pm i\beta$ with positive real part and all other eigenvalues are real and negative. Many classic nonlinear systems have at least one fixed point satisfying this assumption e.g. the Rössler system[28] and the Lorenz system[29]. To analyze the stability of the AD state, we apply standard linear stability analysis to Eq. (1) by considering a small perturbation $\mathbf{x}_i(t) = \mathbf{x}^* + \xi_i(t)$ of the dynamics of the ith node. This results in the variational equation

$$\dot{\xi}_i(t) = DF(\mathbf{x}^*)\xi_i(t) + \sigma \sum_{j=1}^{n} g_{ij}(\xi_j(t-\tau) - \xi_i(t)), \qquad (2)$$

which can be expressed in matrix form as

$$\dot{\xi}(t) = (I_n \otimes (DF(\mathbf{x}^*) - \sigma I_m))\xi(t) + \sigma(G \otimes I_m)\xi(t-\tau), \quad (3)$$

where $\xi = (\xi_1, \xi_2, \ldots, \xi_n)^T$ is the collection of node variations of all nodes in the network and $\otimes$ represents the Kronecker product. Because G is symmetric with positive row sums, there exists an invertible matrix P such that

$$\Gamma = P^{-1}GP = \mathrm{diag}(\gamma_1, \gamma_2, \ldots, \gamma_n), \qquad (4)$$

where the γ_i's are the eigenvalues of G. Applying the change of variables $\xi(t) = (P \otimes I_m)\eta(t)$ to Eq. (3) results in the block diagonalized matrix equation

$$\dot{\eta} = (I_n \otimes (DF(\mathbf{x}^*) - \sigma I_m))\eta(t) + \sigma(\Gamma \otimes I_m)\eta(t-\tau), \quad (5)$$

having n independent modes of the form

$$\dot{\eta}_i = (DF(\mathbf{x}^*) - \sigma)\eta_i(t) + \sigma\gamma_i\eta_i(t-\tau), \qquad (6)$$

for $i = 1, 2, \ldots, n$.

Assuming the initial perturbation of the ith node varies as $\eta_i = e^{\lambda t}$, the stability of the AD state is determined by the characteristic equations

$$\lambda = (\alpha \pm i\beta - \sigma) + \sigma\gamma_i e^{-\lambda\tau}, \qquad (7)$$

for $i = 1, 2, \ldots, n$. The AD state is stable when all of the real parts of the roots of Eq. (7) are negative. Furthermore, it has been shown that the regions of stable AD in the τ-σ parameter space, the ADIs, are enclosed by the four critical curves

$$\begin{aligned}
\tau_1(k,\sigma) &= \frac{2(k-1)\pi + \cos^{-1}\left(\frac{\sigma-\alpha}{\sigma}\right)}{\beta - \sqrt{\sigma^2 - (\sigma-\alpha)^2}},\\
\tau_2(k,\sigma) &= \frac{2k\pi - \cos^{-1}\left(\frac{\sigma-\alpha}{\sigma}\right)}{\beta + \sqrt{\sigma^2 - (\sigma-\alpha)^2}},\\
\tau_3(k,\sigma) &= \frac{2k\pi - \cos^{-1}\left(\frac{\sigma-\alpha}{\sigma\gamma_n}\right)}{\beta - \sqrt{(\sigma\gamma_n)^2 - (\sigma-\alpha)^2}},\\
\tau_4(k,\sigma) &= \frac{2(k-1)\pi + \cos^{-1}\left(\frac{\sigma-\alpha}{\sigma\gamma_n}\right)}{\beta + \sqrt{(\sigma\gamma_n)^2 - (\sigma-\alpha)^2}},
\end{aligned} \qquad (8)$$

where k is an integer corresponding to the island number[16–19,21]. Because each MSI is a composition of ADIs, these critical curves can also be used to generate MSIs.

III. COMPUTING MASTER STABILITY ISLANDS

To compute MSIs using the critical curves from Eq. (8), we choose oscillator dynamics, F, having fixed point $\mathbf{x}^*$, such that $DF(\mathbf{x}^*)$ has conjugate eigenvalues $\alpha \pm i\beta$ with positive real part and all other eigenvalues are real and negative. We then determine the number of MSIs corresponding to the chosen oscillator dynamics. Finally, we use the τ_1 and τ_2 curves to compute the boundary of each MSI and the τ_3 and τ_4 curves to compute the contours inside each MSI.

A. Number of islands

The number of MSIs corresponding to the chosen oscillator dynamics is given by

$$k_{\max} = \left\lfloor \frac{\beta}{\pi\alpha} + \frac{1}{2} \right\rfloor, \qquad (9)$$

where $\lfloor\,\rfloor$ is the floor function[21]. Theoretically, a system could have an arbitrarily large number of MSIs.

B. Island boundaries

The critical curves

$$\tau_1(k,\sigma) = \frac{2(k-1)\pi + \cos^{-1}\left(\frac{\sigma-\alpha}{\sigma}\right)}{\beta - \sqrt{\sigma^2-(\sigma-\alpha)^2}}, \tag{10}$$

and

$$\tau_2(k,\sigma) = \frac{2k\pi - \cos^{-1}\left(\frac{\sigma-\alpha}{\sigma}\right)}{\beta + \sqrt{\sigma^2-(\sigma-\alpha)^2}} \tag{11}$$

depend on the α value and β value of the chosen oscillator dynamics but do not depend on the minimum eigenvalue of the network coupling matrix γ_n. As a result, these curves can be used to compute the boundaries of the MSIs corresponding to the chosen oscillator dynamics in τ-σ parameter space.

The boundary of the kth MSI is found by computing τ_1 and τ_2 between $\sigma = \alpha/2$ and σ_k, where σ_k is found numerically. See Fig. 1. To determine the value of σ_k, we observe that the MSIs corresponding to any chosen oscillator dynamics are bounded above by the function

$$\tau_b(\sigma) = \frac{\pi - \cos^{-1}\left(\frac{\sigma-\alpha}{\sigma}\right)}{\sqrt{\sigma^2-(\sigma-\alpha)^2}}. \tag{12}$$

Moreover, Eq. (12) not only bounds each island, but it also intersects each island at its σ_k value. See Fig. 2. This observation and the fact that σ_k occurs at the delay value $\tau = (2k-1)\pi/\beta$ are used to obtain σ_k by numerically solving the implicit equation $\tau_b(\sigma) = (2k-1)\pi/\beta$ for σ. Because Eq. (12) is a monotonically decreasing function for $\tau \in (0,\infty)$, the MSIs also satisfy $\sigma_k > \sigma_{k+1}$ for $k \geq 1$.

C. Island contours

The critical curves

$$\tau_3(k,\sigma) = \frac{2k\pi - \cos^{-1}\left(\frac{\sigma-\alpha}{\sigma\gamma_n}\right)}{\beta - \sqrt{(\sigma\gamma_n)^2-(\sigma-\alpha)^2}}, \tag{13}$$

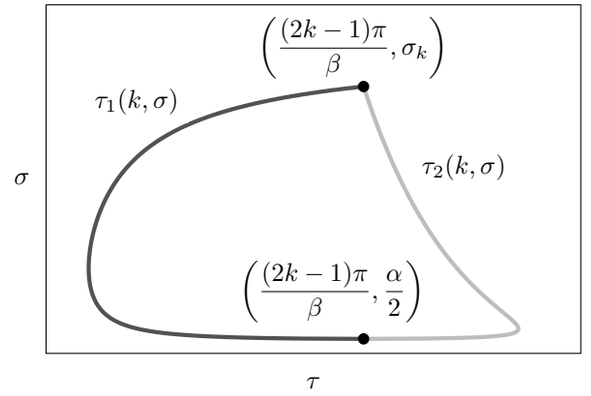

FIG. 1. The boundary of the kth master stability island. The τ_1 and τ_2 curves from Eq. (10) and Eq. (11), respectively, are computed between $\sigma = \alpha/2$ and σ_k.

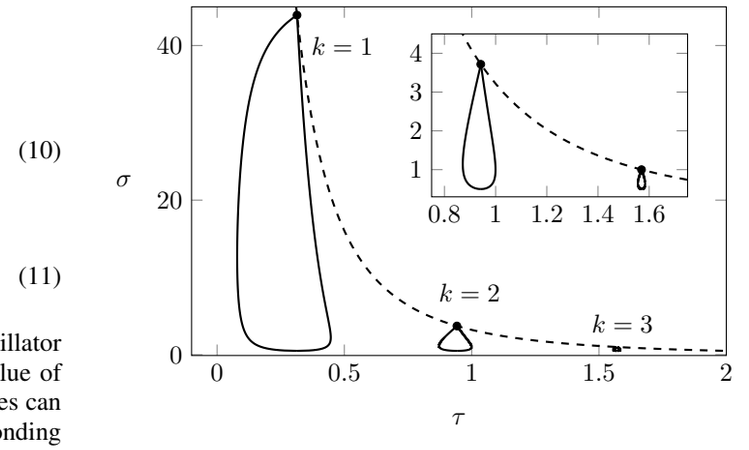

FIG. 2. There are three master stability islands when $\alpha = 1$ and $\beta = 10$. The dashed curve, defined by Eq. (12), intersects each island at its σ_k value.

and

$$\tau_4(k,\sigma) = \frac{2(k-1)\pi + \cos^{-1}\left(\frac{\sigma-\alpha}{\sigma\gamma_n}\right)}{\beta + \sqrt{(\sigma\gamma_n)^2-(\sigma-\alpha)^2}} \tag{14}$$

depend on the α value and β value of the chosen oscillator dynamics as well as on the minimum eigenvalue of the network coupling matrix γ_n. As a result, these curves can be used to compute the contour lines inside each MSI.

Because the kth MSI is defined for $\alpha/2 \leq \sigma \leq \sigma_k$, the τ_3 and τ_4 curves must only be considered over this coupling range. These curves are real-valued for

$$\frac{\alpha}{1-\gamma_n} \leq \sigma \leq \frac{\alpha}{\gamma_n+1},$$

when $\gamma_n \in (-1,0)$. When $\gamma_n = -1$, $\sigma = \alpha/(\gamma_n+1)$ is undefined, and the curves have no maximum coupling value. Because $\alpha/2 \leq \alpha/(1-\gamma_n)$ for $\gamma_n \in [-1,0)$, the range of coupling values where the τ_3 and τ_4 curves can intersect the kth MSI are

$$\frac{\alpha}{1-\gamma_n} \leq \sigma \leq \frac{\alpha}{\gamma_n+1}, \tag{15}$$

if $\alpha/(\gamma_n+1) < \sigma_k$, and

$$\frac{\alpha}{1-\gamma_n} \leq \sigma \leq \sigma_k, \tag{16}$$

if $\alpha/(\gamma_n+1) \geq \sigma_k$. Thus, to add contours to the kth MSI, we choose a subset of γ_n-values in $[-1,0)$ and compute the τ_3 and τ_4 curves inside the MSI using the appropriate coupling interval.

IV. CONTOUR ANALYSIS

When contours are added to the MSIs of a particular oscillator, they create subregions inside them that correspond to

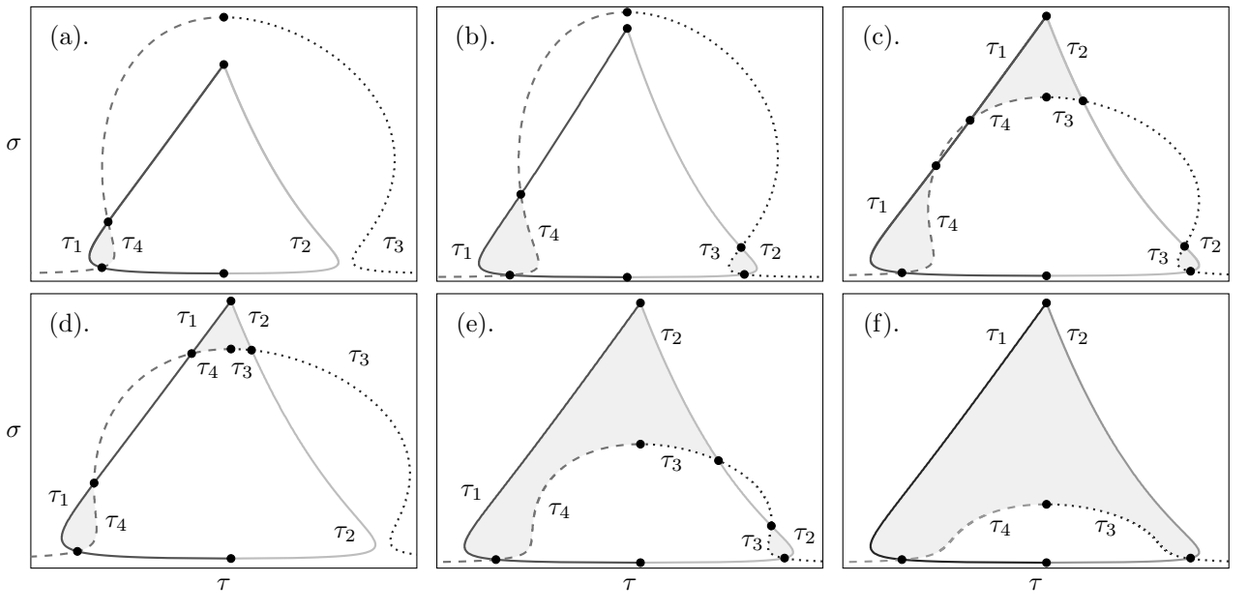

FIG. 3. Examples of the six master stability island contour types. All panels are computed with $k = 2$ and $\alpha = 1$. (a). Type I contours. Computed using $\beta = 29$ and $\gamma_n = -0.98$. (b). Type II contours. Computed using $\beta = 43$ and $\gamma_n = -0.99$. (c). Type III contours. Computed using $\beta = 38$ and $\gamma_n = -0.98$. (d). Type IV contours. Computed using $\beta = 29$ and $\gamma_n = -0.97$. (e). Type V contours. Computed using $\beta = 38$ and $\gamma_n = -0.97$. (f). Type VI contours. Computed using $\beta = 38$ and $\gamma_n = -0.94$.

particular network topologies. In this section, we define contour types as a way to identify the number and form of the MSI subregions that result from any choice of oscillator dynamics and network topology. We also introduce contour sequences and use them to describe the contour types of all MSIs.

A. Contour types

To determine the possible forms of the MSI subregions, we observe that over the coupling intervals given in Eq. (15) and Eq. (16), the τ_3 and τ_4 curves satisfy

$$\tau_4 \leq \frac{(2k-1)\pi}{\beta} \leq \tau_3$$

where $\tau_3 = \tau_4$ only when $\sigma = \alpha/(\gamma_n + 1)$, and the τ_1 and τ_2 curves satisfy

$$\tau_1 \leq \frac{(2k-1)\pi}{\beta} \leq \tau_2$$

where $\tau_1 = \tau_2$ only when $\sigma = \sigma_k$. As a result, τ_4 can intersect τ_1 but it does not intersect τ_2, and τ_3 can intersect τ_2 but it does not intersect τ_1. We find that the intersections of the τ_1 and τ_4 curves and the intersections of the τ_2 and τ_3 curves always satisfy one of the following six cases: (1) The τ_1 and τ_4 curves intersect twice and the τ_2 and τ_3 curves do not intersect. In this case, there is one subregion of stable AD inside the MSI enclosed by the τ_1 and τ_4 curves. See Fig. 3(a). (2) The τ_1 and τ_4 curves intersect twice and the τ_2 and τ_3 curves intersect twice. In this case, there are two subregions of stable AD inside the MSI. One enclosed by the τ_1 and τ_4 curves and one enclosed by the τ_2 and τ_3 curves. See Fig. 3(b). (3) The τ_1 and τ_4 curves intersect three times and the τ_2 and τ_3 curves intersect three times. In this case, there are three subregions of stable AD inside the MSI. One enclosed by the τ_1 and τ_4 curves, one enclosed by the τ_2 and τ_3 curves, and one enclosed by the τ_1, τ_2, τ_3, and τ_4 curves. See Fig. 3(c). (4) The τ_1 and τ_4 curves intersect three times and the τ_2 and τ_3 curves intersect once. In this case, there are two subregions of stable AD inside the MSI. One enclosed by the τ_1 and τ_4 curves and one enclosed by the τ_1, τ_2, τ_3, and τ_4 curves. See Fig. 3(d). (5) The τ_1 and τ_4 curves intersect once and the τ_2 and τ_3 curves intersect three times. In this case, there are two subregions of stable AD inside the MSI. One enclosed by the τ_2 and τ_3 curves and one enclosed by the τ_1, τ_2, τ_3, and τ_4 curves. See Fig. 3(e). (6) The τ_1 and τ_4 curves intersect once and the τ_2 and τ_3 curves intersect once. In this case, there is one subregion of stable AD inside the MSI enclosed by the τ_1, τ_2, τ_3, and τ_4 curves. See Fig. 3(f). Each of these six cases result in different MSI subregion forms that can be identified by how many times τ_1 and τ_4 intersect and how many times τ_2 and τ_3 intersect. As a result, we define each contour type as an ordered pair (I_{14}, I_{23}), where I_{14} is the number of intersections of the τ_1 and τ_4 curves and I_{23} is the number of intersections of the τ_2 and τ_3 curves. Therefore, contours satisfying cases one through six are defined by the ordered pairs $(2,0)$, $(2,2)$, $(3,3)$, $(3,1)$, $(1,3)$, and $(1,1)$, respectively. For ease of reference, we call contours that satisfy case one, Type I contours, contours that satisfy case two, Type II contours, and so on. To confirm that these six MSI contour types are the only possible contour types, we now show that for any choice of k, α, β, and γ_n the number of intersections of the τ_1 and τ_4 curves and

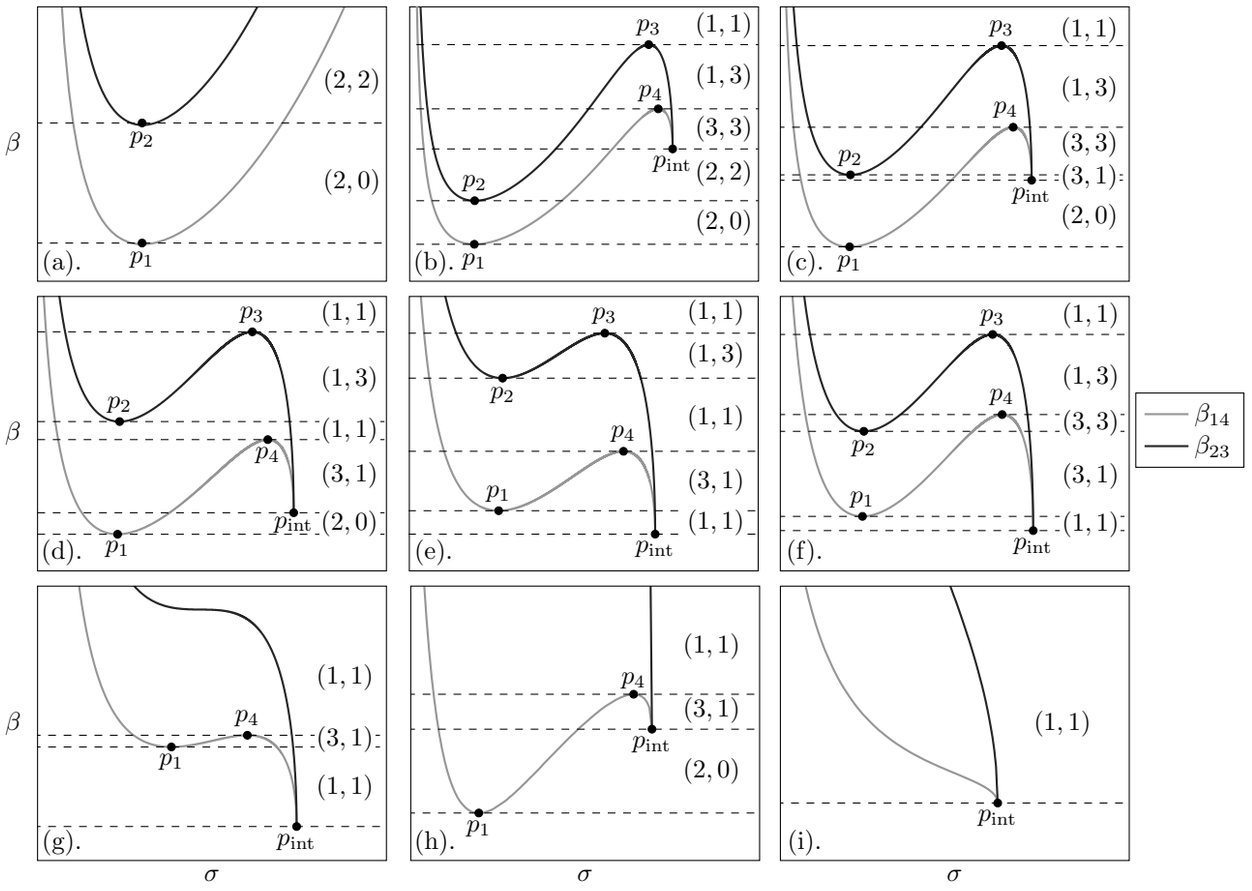

FIG. 4. Examples of the nine possible β-axis partitions and resulting ordered pairs of the number of intersections of the τ_1 and τ_4 curves and the τ_2 and τ_3 curves. In each panel, the β_{14} and β_{23} curves are computed with $\alpha = 1$ using Eq. (17) and Eq. (18), respectively. (a). Computed with $k = 2$ and $\gamma_n = -1$. (b). Computed with $k = 2$ and $\gamma_n = -0.997$. (c). Computed with $k = 2$ and $\gamma_n = -0.98$. (d). Computed with $k = 2$ and $\gamma_n = -0.965$. (e). Computed with $k = 2$ and $\gamma_n = -0.95$. (f). Computed with $k = 3$ and $\gamma_n = -0.962$. (g). Computed with $k = 2$ and $\gamma_n = -0.92$. (h). Computed with $k = 1$ and $\gamma_n = -0.87$. (i). Computed with $k = 1$ and $\gamma_n = -0.6$.

the number of intersections of the τ_2 and τ_3 curves will always be given by one of these six ordered pairs.

To find the intersections of the τ_1 and τ_4 curves, we set $\tau_1 = \tau_4$ and solve for β to obtain the curve

$$\beta_{14} = \frac{\left[2\pi(k-1) + \cos^{-1}\left(\frac{\sigma-\alpha}{\sigma}\right)\right]\sqrt{(\sigma\gamma_n)^2 - (\sigma-\alpha)^2}}{\cos^{-1}\left(\frac{\sigma-\alpha}{\sigma\gamma_n}\right) - \cos^{-1}\left(\frac{\sigma-\alpha}{\sigma}\right)} + \frac{\left[2\pi(k-1) + \cos^{-1}\left(\frac{\sigma-\alpha}{\sigma\gamma_n}\right)\right]\sqrt{(\sigma)^2 - (\sigma-\alpha)^2}}{\cos^{-1}\left(\frac{\sigma-\alpha}{\sigma\gamma_n}\right) - \cos^{-1}\left(\frac{\sigma-\alpha}{\sigma}\right)}, \tag{17}$$

and to find the intersections of the τ_2 and τ_3 curves, we set $\tau_2 = \tau_3$ and solve for β to obtain the curve

$$\beta_{23} = \frac{\left[2\pi k - \cos^{-1}\left(\frac{\sigma-\alpha}{\sigma}\right)\right]\sqrt{(\sigma\gamma_n)^2 - (\sigma-\alpha)^2}}{\cos^{-1}\left(\frac{\sigma-\alpha}{\sigma\gamma_n}\right) - \cos^{-1}\left(\frac{\sigma-\alpha}{\sigma}\right)} + \frac{\left[2\pi k - \cos^{-1}\left(\frac{\sigma-\alpha}{\sigma\gamma_n}\right)\right]\sqrt{(\sigma)^2 - (\sigma-\alpha)^2}}{\cos^{-1}\left(\frac{\sigma-\alpha}{\sigma\gamma_n}\right) - \cos^{-1}\left(\frac{\sigma-\alpha}{\sigma}\right)}. \tag{18}$$

For fixed values of k, α, β, and γ_n, the number of intersections of the τ_1 and τ_4 curves and the τ_2 and τ_3 curves is given by the number of σ-values satisfying Eq. (17) and Eq. (18), respectively. For $\gamma_n \in (-1,0)$, these curves are defined over the domain

$$\frac{\alpha}{2} < \sigma \leq \frac{\alpha}{\gamma_n + 1},$$

the curves satisfy that $\beta_{14} < \beta_{23}$ on the interior of this domain, and $\beta_{14} = \beta_{23}$ at the right endpoint

$$p_{\text{int}} = \left(\frac{\alpha}{1+\gamma_n}, \frac{\alpha(2k-1)\pi\sqrt{\frac{1-\gamma_n}{1+\gamma_n}}}{\cos^{-1}(\gamma_n)}\right).$$

When $\gamma_n = -1$, the domain of each curve is reduced to

$$\frac{\alpha}{2} < \sigma < \frac{\alpha}{\gamma_n + 1}$$

because p_{int} is undefined; however, it is still the case that $\beta_{14} < \beta_{23}$ on the interior of this domain. We numerically determine that, over either domain, there are always one, two,

or three values of σ satisfying Eq. (17) and Eq. (18), and because $\beta_{14} < \beta_{23}$ on the interior of either domain, the ordered pairs representing the number of intersections of the τ_1 and τ_4 curves and the number of intersections of the τ_2 and τ_3 curves can only contain the integers 0, 1, 2, or 3.

To find all valid ordered pairs of intersections, we compute the β_{14} and β_{23} curves in σ-β space using fixed values of k, α, and γ_n and identify the extreme values of each curve. These values are then used to partition the β-axis so that each interval corresponds to one ordered pair, where no adjacent intervals have the same ordered pair. When $\gamma_1 = -1$, each curve has a global minimum, and we denote the extreme value on the β_{14} curve by p_1 and the extreme value on the β_{23} curve by p_2. Fig. 4(a). shows the curves, the extreme values, and the resulting ordered pairs of intersections. For $\gamma_n \in (-1,0)$, both curves always have one extreme value at p_{int}, and depending on the value of γ_n, satisfy one of the following cases: (1) The β_{14} curve has two more extreme values and the β_{23} curve has two more extreme values. (2) The β_{14} curve has two more extreme values and the β_{23} curve has no more extreme values. When the β_{14} curve has two more extreme values, we denote these points by p_1 and p_4, where $p_1 < p_4$ with respect to β, and when the β_{23} curve has two more extreme values, we denote these points by p_2 and p_3, where $p_2 < p_3$ with respect to β. Because $\beta_{14} < \beta_{23}$ with respect to β for all

$$\alpha/2 < \sigma < \frac{\alpha}{\gamma_n + 1},$$

it also follows that $p_1 < p_2$ and $p_4 < p_3$ with respect to β. Using these inequalities, and the fact that $p_{\text{int}} < p_4$ with respect to β, we are able to determine that the resulting partitions must have one of the eight forms shown in Fig. 4(b)-(i). In each of the nine cases shown in Fig. 4, the partitions are made up of one or more of the six ordered pairs of intersections corresponding to the six contour types. This confirms the six MSI contour types.

B. Contour dependence on α, β, and γ_n

The β_{14} curve and the β_{23} curve given by Eq. (17) and Eq. (18), respectively, depend on four parameters: k, α, β, and γ_n. For any fixed island number k, these curves can be used to determine the contour type corresponding to all values of α, β, and γ_n. Each $\gamma_n \in [-1,0)$ corresponds to a valid ordering of a subset of the points p_1, p_4, p_2, p_3, and p_{int} with respect to the β-axis, that is, each value of γ_n corresponds to one of the nine cases shown in Fig. 4.

As a result, these points can be used to partition β-γ_n space into regions of distinct contour type by computing each point as a function of γ_n. This generates boundary curves for each region of distinct contour type and Fig. 5 shows these regions for the first three generic MSIs. In our numerical simulations, we find that the β-values of the resulting regions scale linearly with respect to α. Thus, the β-axis in Fig. 5 can be given in terms of α, and the regions given in Fig. 5 provide the resulting contour type for any α, β, and γ_n.

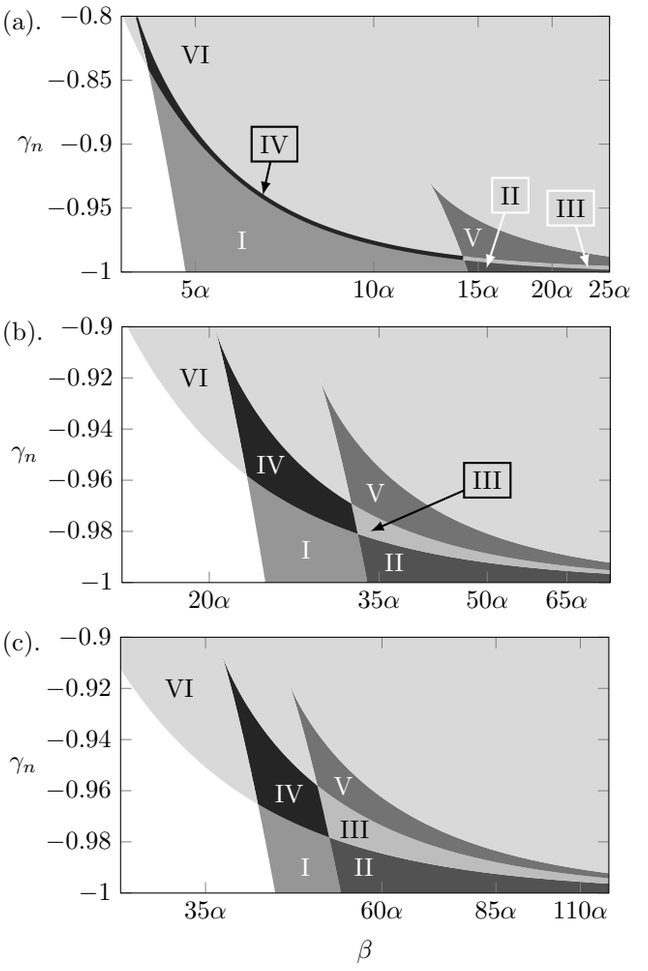

FIG. 5. Contour type regions computed using Eq. (17) and Eq. (18) with $\alpha = 1$. The white region in $\alpha\beta$-γ_n space is where the contour curves do not intersect the master stability island in τ-σ space. (a). Contour regions for the generic master stability island one. (b). Contour regions for the generic master stability island two. (c). Contour regions for the generic master stability island three.

C. Contour sequences

To determine the contour type makeup of all MSIs, we define horizontal and vertical contour sequences. Horizontal contour sequences correspond to a fixed γ_n value and vertical contour sequences correspond to a fixed $\alpha\beta$ value. There are nine unique horizontal contour sequences and seven unique vertical contour sequences given in Table I, and these were determined numerically by tracking the points p_1, p_4, p_2, p_3, and p_{int} in $\alpha\beta$-γ_n space. Note that each horizontal contour sequence corresponds to one panel in Fig. 4. Table II and Table III provide γ_n intervals and $\alpha\beta$ intervals for the first three generic MSIs corresponding to horizontal contour sequences and vertical contour sequences, respectively.

We use the horizontal contour sequences to examine the contour type of each generic MSI. Fig. 6 shows the γ_n inter-

Horizontal Contour Sequences	Vertical Contour Sequences
H_1: I, II	V_1: I, IV, VI
H_2: I, II, III, V, VI	V_2: I, II, III, V, VI
H_3: I, IV, III, V, VI	V_3: I, IV, III, V, VI
H_4: I, IV, VI	V_4: I, IV, VI, V, VI
H_5: I, IV, VI, V, VI	V_5: II, III, V, VI
H_6: VI	V_6: VI
H_7: VI, IV, III, V, VI	V_7: VI, IV, VI
H_8: VI, IV, VI	
H_9: VI, IV, VI, V, VI	

TABLE I. There are seven unique vertical contour sequences and nine unique horizontal contour sequences.

Island	γ_n Interval	Horizontal Sequence
k=1	$\{-1\}$	H_1
	$(-1,-0.9890)$	H_2
	$[-0.9890,-0.9286)$	H_5
	$[-0.9286,-0.8409)$	H_4
	$[-0.8409,-0.8001)$	H_8
	$[-0.8001,0)$	H_6
k=2	$\{-1\}$	H_1
	$(-1,-0.9809)$	H_2
	$[-0.9809,-0.9691)$	H_3
	$[-0.9691,-0.9582)$	H_5
	$[-0.9582,-0.9205)$	H_9
	$[-0.9205,-0.9005)$	H_8
	$[-0.9005,0)$	H_6
k=3	$\{-1\}$	H_1
	$(-1,-0.9782)$	H_2
	$[-0.9782,-0.9652)$	H_3
	$[-0.9652,-0.9579)$	H_7
	$[-0.9579,-0.9180)$	H_9
	$[-0.9180,-0.9065)$	H_8
	$[-0.9065,0)$	H_6

TABLE II. Horizontal contour sequences with corresponding γ_n intervals. All intervals were computed using Eq (17) and Eq (18) with $\alpha = 1$.

vals and corresponding horizontal contour sequences for the first twenty generic MSIs. We find that as γ_n is increased from $\gamma_n = -1$ to $\gamma_n = 0$, the first generic MSI has the horizontal contour sequence ordering H_1, H_2, H_5, H_4, H_8, and H_6, the second generic MSI has the horizontal contour sequence ordering H_1, H_2, H_3, H_5, H_9, H_8, and H_6, and the third generic MSI has the horizontal contour sequence ordering H_1, H_2, H_3, H_7, H_9, H_8, and H_6. Fig. 6 shows that all subsequent generic MSIs have the same horizontal contour sequence ordering as the third generic MSI and that the γ_n intervals corresponding to the horizontal contour sequences H_3, H_8, and H_9 decrease in size as the island number increases.

When computing MSIs, the values of α and β are fixed by the choice of oscillator dynamics and system parameters. As a result, vertical contour sequences can be used to determine which γ_n values should be chosen when computing MSI contours. To produce a visually useful MSI, the chosen γ_n values should produce contours from each of the different contour

Island	β Interval	Vertical Sequence
k=1	$(1.5708\alpha, 3.9639\alpha)$	V_6
	$[3.9639\alpha, 4.1493\alpha)$	V_7
	$[4.1493\alpha, 12.3762\alpha)$	V_1
	$[12.3762\alpha, 14.1562\alpha)$	V_4
	$[14.1562\alpha, 14.1756\alpha)$	V_3
	$[14.1756\alpha, 14.4124\alpha)$	V_2
	$[14.4124\alpha, \infty)$	V_5
k=2	$(4.724\alpha, 20.3709\alpha)$	V_6
	$[20.3709\alpha, 22.6328\alpha)$	V_7
	$[22.63.28\alpha, 28.7723\alpha)$	V_1
	$[28.7723\alpha, 31.9452\alpha)$	V_4
	$[31.9452\alpha, 32.6256\alpha)$	V_3
	$[32.6256\alpha, 33.6335\alpha)$	V_2
	$[33.6335\alpha, \infty)$	V_5
k=3	$(7.8540\alpha, 36.7610\alpha)$	V_6
	$[36.7610\alpha, 41.0788\alpha)$	V_7
	$[41.0788\alpha, 45.1657\alpha)$	V_1
	$[45.1657\alpha, 49.2495\alpha)$	V_4
	$[49.2495\alpha, 51.0720\alpha)$	V_3
	$[51.0720\alpha, 52.8547\alpha)$	V_2
	$[52.8547\alpha, \infty)$	V_5

TABLE III. Vertical contour sequences with corresponding $\alpha\beta$ intervals for the first three master stability islands. All intervals were computed using Eq (17) and Eq (18) with $\alpha = 1$.

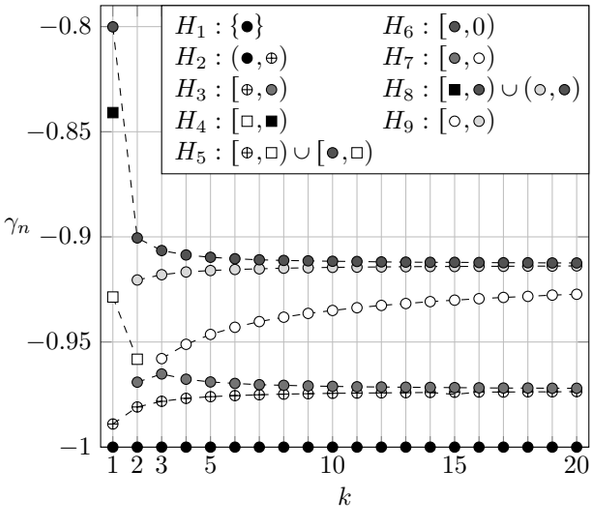

FIG. 6. Horizontal contour sequence intervals for the first twenty generic master stability islands.

type regions known to exist within the island. Fig. 7 shows the $\alpha\beta$ intervals and corresponding vertical contour sequences for the first fifteen generic MSIs. We find that all MSIs have the same vertical contour sequence ordering V_6, V_7, V_1, V_4, V_3, V_2, and V_5 as $\alpha\beta$ increases from $(2k+1)\pi/2$, and that the $\alpha\beta$ interval of each vertical contour sequence increases as the island number increases.

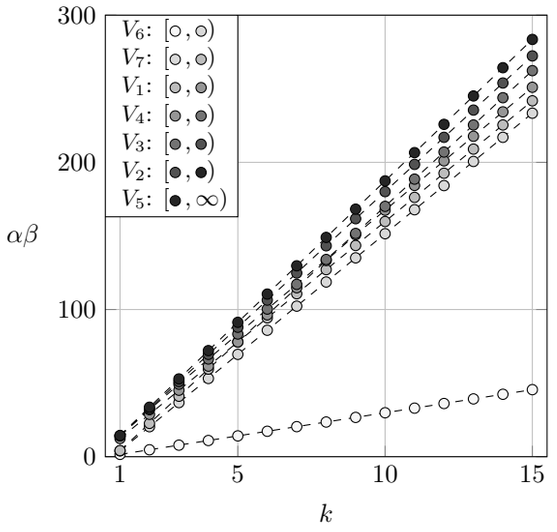

FIG. 7. Vertical contour sequence intervals for the first fifteen generic master stability islands.

V. EXAMPLES

A. van der Pol

The van der Pol system[30] is given by

$$\begin{cases} \dot{x} &= y, \\ \dot{y} &= -x+\mu(1-x^2)y. \end{cases} \tag{19}$$

When $\mu = 0.1$, this system has an unstable fixed point at the origin, and its Jacobian matrix

$$DF = \begin{bmatrix} 0 & 1 \\ -1-2\mu x^* y^* & \mu(1-(x^*)^2) \end{bmatrix}$$

evaluated at this fixed point has eigenvalues $\lambda_{1,2} \simeq 0.05 \pm 0.9987i$. Thus, $\alpha = 0.05$ and $\beta = 0.9987$, and the van der Pol system with $\mu = 0.1$ has

$$\left\lfloor \frac{0.9987}{\pi(0.05)} + \frac{1}{2} \right\rfloor = 6$$

Island	Contour Type	γ_n Interval
$k=1$	II	$[-1,-0.99465)$
	III	$[-0.99465,-0.99464)$
	V	$[-0.99464,-0.97976)$
	VI	$[-0.97976,0)$
$k=2$	VI	$[-0.9451,0)$
$k=3$	VI	$[-0.82522,0)$
$k=4$	VI	$[-0.60554,0)$
$k=5$	VI	$[-0.2456,0)$
$k=6$	VI	$[0.3102,1]$

TABLE IV. Contour types and γ_n intervals of the six van der Pol master stability islands.

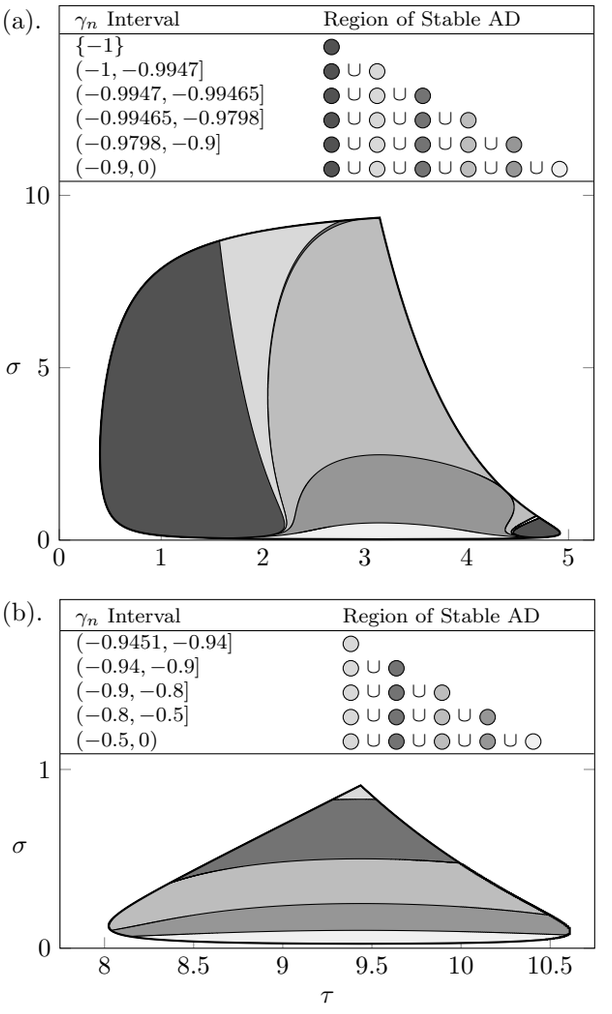

FIG. 8. (a). Van der Pol master stability island one. (b). Van der Pol master stability island two.

MSIs. The first MSI has vertical contour sequence V_5 and the five other MSIs have vertical contour sequence V_6. The contour types and corresponding γ_n intervals for all six MSIs are given in Table IV. Because the sixth MSI has a γ_n interval of positive values, this island will not have a region of stable amplitude death for the networks under study. The first two MSIs are given in Fig. 8. The four other MSIs have the same form as the second MSI and are not included here.

B. Rucklidge system

The Rucklidge system[31] is given by

$$\begin{cases} \dot{x} &= -ax+by-yz, \\ \dot{y} &= x, \\ \dot{z} &= -z+y^2. \end{cases} \tag{20}$$

Island	Contour Type	γ_n Interval
$k=1$	VI	$[-0.72914, 0)$

TABLE V. Contour type and γ_n interval of the Rucklidge master stability island.

When $a=-0.1$ and $b=0.1$, this system has a fixed point at $x^*=0$, $y^*\simeq 0.3162$, and $z^*\simeq 0.1$, and its Jacobian matrix

$$DF=\begin{bmatrix}-a & b-z & -y\\ 1 & 0 & 0\\ 0 & 2y & -1\end{bmatrix} \tag{21}$$

evaluated at this fixed point has eigenvalues $\mu_1\simeq 0.1206+0.4009i$, $\mu_2\simeq 0.1206-0.4009i$, and $\mu_3\simeq -1.1412$. Thus, $\alpha=0.1206$ and $\beta=0.4009$, and the Rucklidge system has

$$\left\lfloor \frac{0.1206}{\pi(0.4009)}+\frac{1}{2}\right\rfloor = 1$$

MSI. The MSI has vertical contour sequence V_6 and the contour types and corresponding γ_n intervals are given in Table V. The Rucklidge MSI is given in Fig. 9.

C. Rössler system

The Rössler system[28] is given by

$$\begin{cases}\dot{x} &= -y-z,\\ \dot{y} &= x+ay,\\ \dot{z} &= b+(x-c)z.\end{cases} \tag{22}$$

When $a=0.15$, $b=0.2$, and $c=10$, this system has a fixed point at $x^*\simeq 0.003$, $y^*\simeq -0.02$ and $z^*\simeq 0.02$, and its Jacobian matrix

$$DF=\begin{bmatrix}0 & -1 & -1\\ 1 & a & 0\\ z & 0 & x-c\end{bmatrix}$$

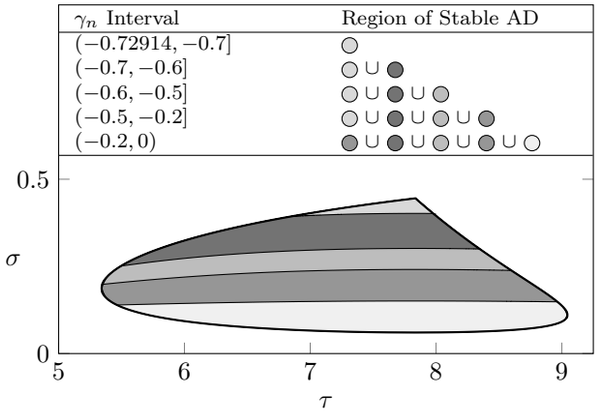

FIG. 9. Rucklidge master stability island.

Island	Contour Type	γ_n Interval
$k=1$	I	$[-1, -0.98788)$
	IV	$[-0.98788, -0.98784)$
	VI	$[-0.98784, -0.985)$
	V	$[-0.985, -0.96386)$
	VI	$[-0.96386, 0)$
$k=2$	VI	$[-0.86694, 0)$
$k=3$	VI	$[-0.54457, 0)$
$k=4$	VI	$[0.11148, 1]$

TABLE VI. Contour types and γ_n intervals of the four Rössler master stability islands.

evaluated at this fixed point has eigenvalues $\lambda_{1,2}\simeq 0.0740\pm 0.9972i$ and $\lambda_3\simeq -9.9950$. Thus, $\alpha=0.0740$ and $\beta=0.9972$, and the Rössler system has

$$\left\lfloor \frac{0.9972}{\pi(0.0740)}+\frac{1}{2}\right\rfloor = 4$$

MSIs. The first MSI has vertical contour sequence V_4 and the three other MSIs have vertical contour sequence V_6. The contour types and corresponding γ_n intervals given in Table VI. Because the fourth MSI has a γ_n interval of positive values, this island will not have a region of stable amplitude death for the networks under study. The first three Rössler system MSIs are not given here but can be found in[26].

VI. CONCLUSIONS

In this paper, we presented a method to compute MSIs for amplitude death in networks of delay-coupled oscillators using critical curves and provided several examples of nonlinear systems and their MSIs. We analyzed the effects of the oscillator dynamics and the network topology on the number, size, and contour types of the MSIs, and used this analysis to determine the contour make-up of all MSIs. Many articles only report on the region of stable AD that is a subregion of the first MSI, but using contour types and contour sequences we were able to analyze all possible MSIs, and hence, all possible ADIs for any choice of oscillator dynamics and network topology.

Studies of AD in networks of delay-coupled oscillators report that the number of ADIs in τ-σ space and their corresponding sizes depend on the oscillator dynamics and the network topology[16–24,26]. It has also been shown that the ADIs corresponding to an oscillator are minimized or maximized in size when $\gamma_n\in[-1,0)$ is minimized or maximized, respectively[21]. Because MSIs are made up of ADIs, this relationship holds true in the MSI framework. This increase in the size of the region of stable AD as γ_n increases is observed in Fig. 8 and in Fig. 9.

ACKNOWLEDGMENTS

We acknowledge an internal research grant from Fairleigh Dickinson University.

[1]D. G. Aronson, G. B. Ermentrout, and N. Kopell, "Amplitude response of coupled oscillators," Physica D: Nonlinear Phenomena **41**, 403–449 (1990).
[2]R. E. Mirollo and S. H. Strogatz, "Amplitude death in an array of limit-cycle oscillators," Journal of Statistical Physics **60**, 245–262 (1990).
[3]F. M. Atay, "Distributed delays facilitate amplitude death of coupled oscillators," Phys. Rev. Lett. **91**, 094101 (2003).
[4]K. Konishi, "Amplitude death induced by dynamic coupling," Phys. Rev. E **68**, 067202 (2003).
[5]K. Konishi, "Amplitude death in oscillators coupled by a one-way ring time-delay connection," Phys. Rev. E **70**, 066201 (2004).
[6]A. Prasad, "Amplitude death in coupled chaotic oscillators," Phys. Rev. E **72**, 056204 (2005).
[7]R. Karnatak, R. Ramaswamy, and A. Prasad, "Amplitude death in the absence of time delays in identical coupled oscillators," Phys. Rev. E **76**, 035201 (2007).
[8]W. Liu, X. Wang, S. Guan, and C.-H. Lai, "Transition to amplitude death in scale-free networks," New Journal of Physics **11**, 093016 (2009).
[9]A. Prasad, M. Dhamala, B. M. Adhikari, and R. Ramaswamy, "Amplitude death in nonlinear oscillators with nonlinear coupling," Phys. Rev. E **81**, 027201 (2010).
[10]V. Resmi, G. Ambika, and R. E. Amritkar, "General mechanism for amplitude death in coupled systems," Phys. Rev. E **84**, 046212 (2011).
[11]L. B. Le, K. Konishi, and N. Hara, "Topology-free design for amplitude death in time-delayed oscillators coupled by a delayed connection," Phys. Rev. E **87**, 042908 (2013).
[12]A. Gjurchinovski, A. Zakharova, and E. Schöll, "Amplitude death in oscillator networks with variable-delay coupling," Phys. Rev. E **89**, 032915 (2014).
[13]W. Zou, M. Zhan, and J. Kurths, "Amplitude death in globally coupled oscillators with time-scale diversity," Phys. Rev. E **98**, 062209 (2018).
[14]Z. Sun, N. Zhao, X. Yang, and W. Xu, "Inducing amplitude death via discontinuous coupling," Nonlinear Dynamics **92**, 1185–1195 (2018).
[15]A. K. Singh and R. S. Yadava, "Synchronization and amplitude death in a pair of van der pol oscillators under conjugate coupling," Physica Scripta (2019).
[16]D. V. Ramana Reddy, A. Sen, and G. L. Johnston, "Time delay induced death in coupled limit cycle oscillators," Phys. Rev. Lett. **80**, 5109–5112 (1998).
[17]D. R. Reddy, A. Sen, and G. L. Johnston, "Time delay effects on coupled limit cycle oscillators at hopf bifurcation," Physica D: Nonlinear Phenomena **129**, 15–34 (1999).
[18]R. Dodla, A. Sen, and G. L. Johnston, "Phase-locked patterns and amplitude death in a ring of delay-coupled limit cycle oscillators," Phys. Rev. E **69**, 056217 (2004).
[19]P. Hövel and E. Schöll, "Control of unstable steady states by time-delayed feedback methods," Physical Review E **72**, 046203 (2005).
[20]W. Zou and M. Zhan, "Partial time-delay coupling enlarges death island of coupled oscillators," Phys. Rev. E **80**, 065204 (2009).
[21]W. Zou, X. Zheng, and M. Zhan, "Insensitive dependence of delay-induced oscillation death on complex networks," Chaos: An Interdisciplinary Journal of Nonlinear Science **21**, 023130 (2011).
[22]W. Zou, D. V. Senthilkumar, Y. Tang, Y. Wu, J. Lu, and J. Kurths, "Amplitude death in nonlinear oscillators with mixed time-delayed coupling," Phys. Rev. E **88**, 032916 (2013).
[23]R. Nagao, W. Zou, J. Kurths, and I. Z. Kiss, "Restoring oscillatory behavior from amplitude death with anti-phase synchronization patterns in networks of electrochemical oscillations," Chaos: An Interdisciplinary Journal of Nonlinear Science **26**, 094808 (2016).
[24]R. Xiao, Z. Sun, X. Yang, and W. Xu, "Emergence of death islands in fractional-order oscillators via delayed coupling," Communications in Nonlinear Science and Numerical Simulation **69**, 168–175 (2019).
[25]S. Huddy and J. Skufca, "Amplitude death solutions for stabilization of dc microgrids with instantaneous constant-power loads," Power Electronics, IEEE Transactions on **28**, 247 –253 (2013).
[26]S. R. Huddy and J. Sun, "Master stability islands for amplitude death in networks of delay-coupled oscillators," Phys. Rev. E **93**, 052209 (2016).
[27]W. Michiels and H. Nijmeijer, "Synchronization of delay-coupled nonlinear oscillators: An approach based on the stability analysis of synchronized equilibria," Chaos: An Interdisciplinary Journal of Nonlinear Science **19**, 033110 (2009).
[28]O. Rössler, "An equation for continuous chaos," Physics Letters A **57**, 397 – 398 (1976).
[29]E. N. Lorenz, "Deterministic nonperiodic flow," Journal of the atmospheric sciences **20**, 130–141 (1963).
[30]B. Van der Pol, "A theory of the amplitude of free and forced triode vibrations," Radio Review **1**, 701–710 (1920).
[31]A. Rucklidge, "Chaos in models of double convection," Journal of Fluid Mechanics **237**, 209–229 (1992).
[32]G. Chen and T. Ueta, "Yet another chaotic attractor," International Journal of Bifurcation and Chaos **9**, 1465–1466 (1999).
[33]T. Rikitake, "Oscillations of a system of disk dynamos," in *Mathematical Proceedings of the Cambridge Philosophical Society*, Vol. 54 (Cambridge University Press, 1958) pp. 89–105.
[34]M. Rabinovich and A. Fabrikant, "Stochastic self-modulation of waves in nonequilibrium media," Journal of Experimental and Theoretical Physics **77**, 617–629 (1979).
[35]J. C. Sprott, "Some simple chaotic flows," Phys. Rev. E **50**, R647–R650 (1994).
[36]J. C. Sprott, X. Wang, and G. Chen, "Coexistence of point, periodic and strange attractors," International Journal of Bifurcation and Chaos **23**, 1350093 (2013).
[37]T. Shimizu and N. Morioka, "On the bifurcation of a symmetric limit cycle to an asymmetric one in a simple model," Physics Letters A **76**, 201–204 (1980).
[38]T. Matsumoto, L. O. Chua, and M. Komuro, *Bifurcation phenomena in a third order electrical circuit* (Electronics Research Laboratory, College of Engineering, University of California, 1985).
[39]S. Wiggins, "Application to the dynamics of the damped, forced duffing oscillator," Introduction to Applied Nonlinear Dynamical Systems and Chaos. New York: Springer-Verlag (1990).
[40]T. Nishikawa and A. E. Motter, "Network synchronization landscape reveals compensatory structures, quantization, and the positive effect of negative interactions," Proceedings of the National Academy of Sciences **107**, 10342–10347 (2010).
[41]B. Ravoori, A. B. Cohen, J. Sun, A. E. Motter, T. E. Murphy, and R. Roy, "Robustness of optimal synchronization in real networks," Physical review letters **107**, 034102 (2011).
[42]P. S. Skardal, D. Taylor, and J. Sun, "Optimal synchronization of complex networks," Physical review letters **113**, 144101 (2014).
[43]P. S. Skardal, D. Taylor, and J. Sun, "Optimal synchronization of directed complex networks," Chaos: An Interdisciplinary Journal of Nonlinear Science **26**, 094807 (2016).
[44]T. Nishikawa, J. Sun, and A. E. Motter, "Sensitive dependence of optimal network dynamics on network structure," Physical Review X **7**, 041044 (2017).
[45]M. P. Mehta and A. Sen, "Death island boundaries for delay-coupled oscillator chains," Physics Letters A **355**, 202–206 (2006).

PLEASE CITE THIS ARTICLE AS DOI: 10.1063/1.5121029

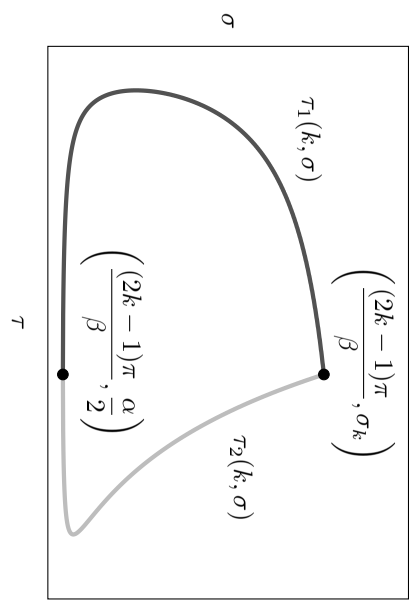

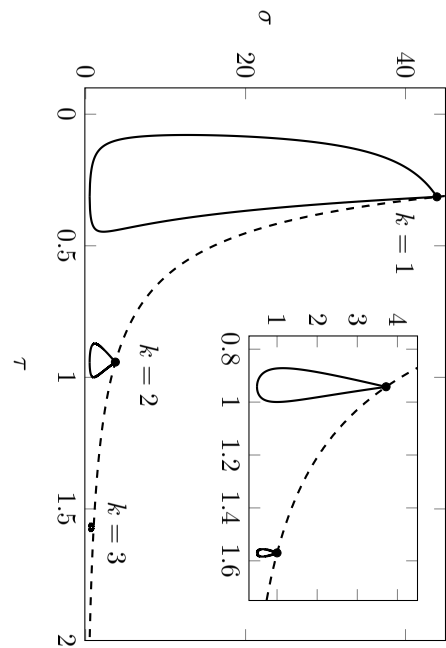

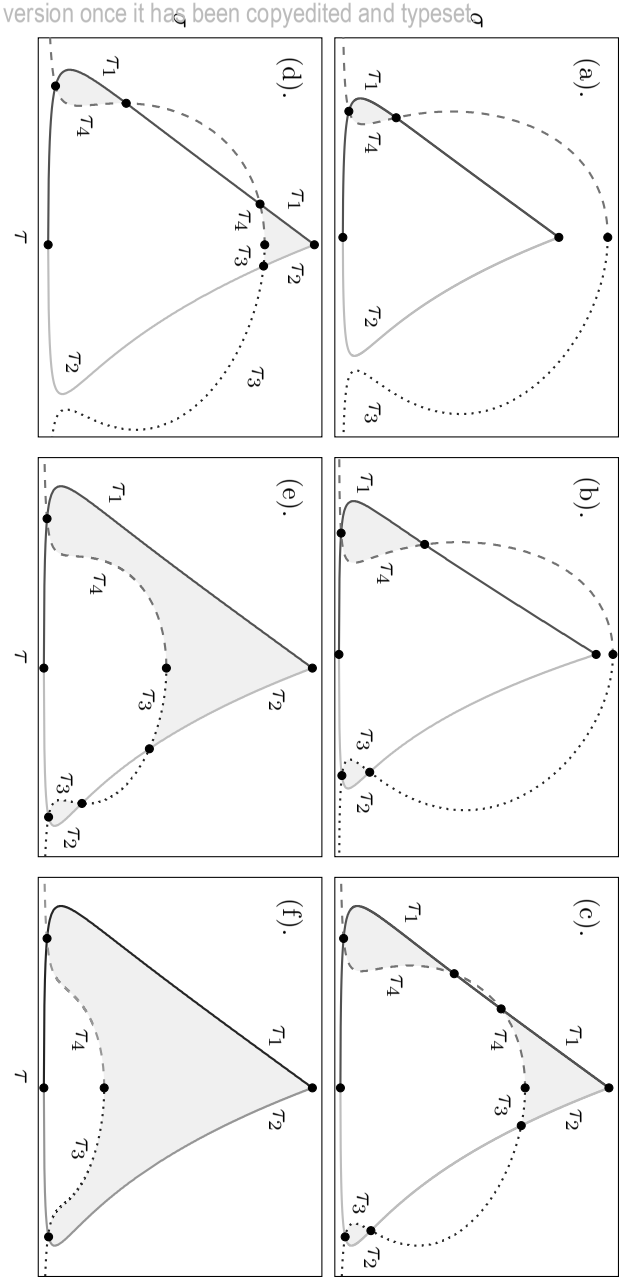

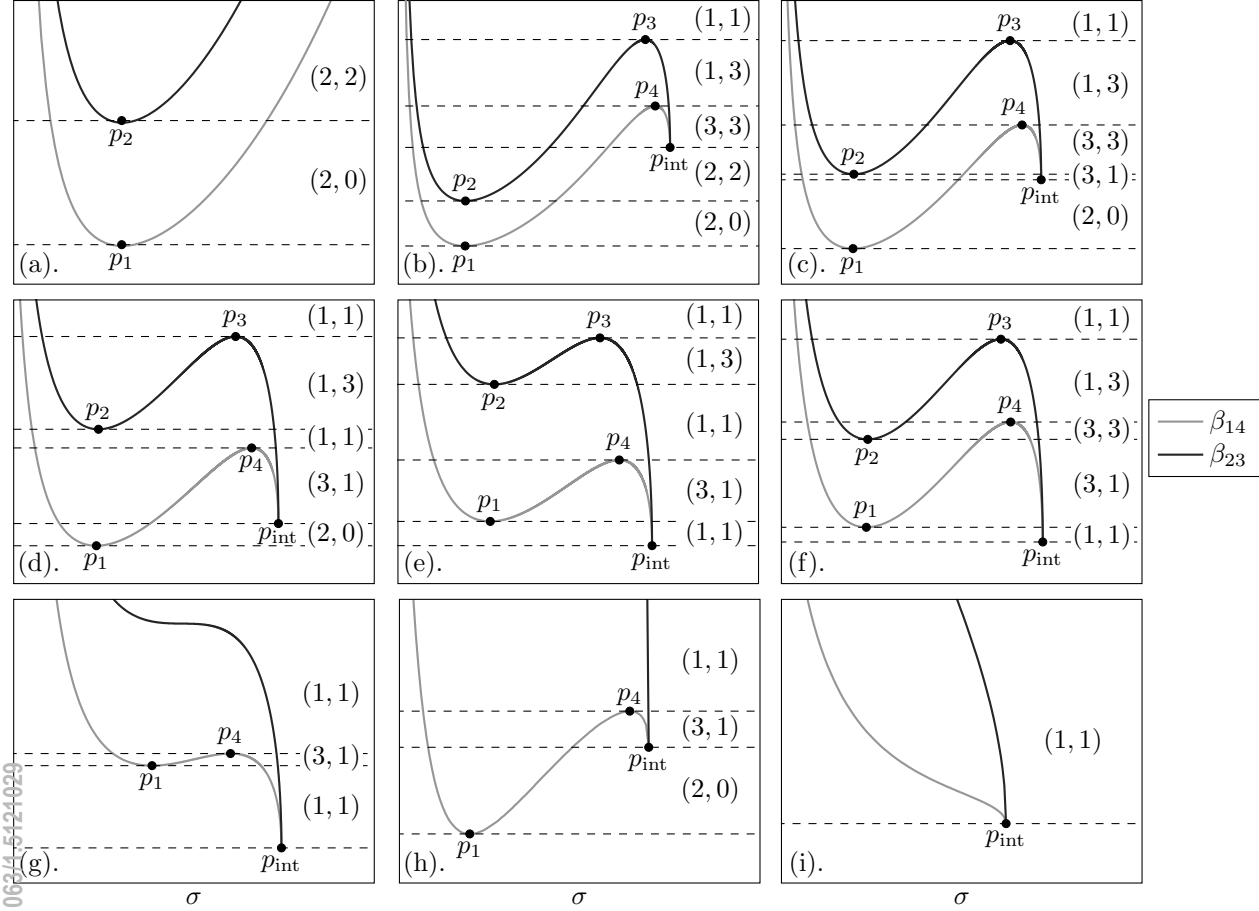

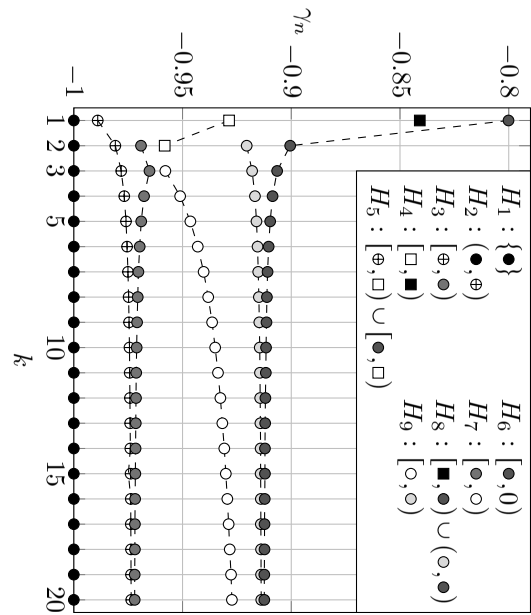

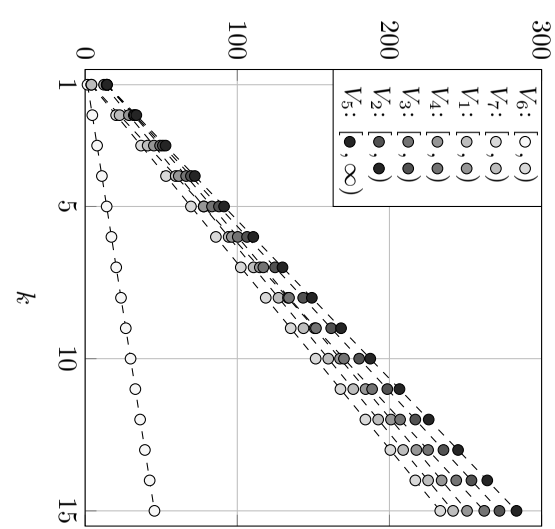

(a).

γ_n Interval	Region of Stable AD
$\{-1\}$	●
$(-1, -0.9947]$	● ∪ ○
$(-0.9947, -0.99465]$	● ∪ ○ ∪ ●
$(-0.99465, -0.9798]$	● ∪ ○ ∪ ● ∪ ○
$(-0.9798, -0.9]$	● ∪ ○ ∪ ● ∪ ○ ∪ ●
$(-0.9, 0)$	● ∪ ○ ∪ ● ∪ ○ ∪ ● ∪ ○

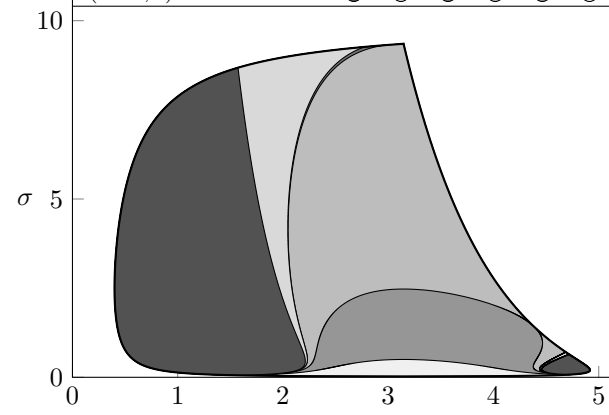

(b).

γ_n Interval	Region of Stable AD
$(-0.9451, -0.94]$	○
$(-0.94, -0.9]$	○ ∪ ●
$(-0.9, -0.8]$	○ ∪ ● ∪ ○
$(-0.8, -0.5]$	○ ∪ ● ∪ ○ ∪ ●
$(-0.5, 0)$	○ ∪ ● ∪ ○ ∪ ● ∪ ○